Proton and deuteron production in Au+Au reactions at 11.6*A* GeV/*c*

L. Ahle,[9,*] Y. Akiba,[6] K. Ashktorab,[1] M. D. Baker,[9,†] D. Beavis,[1] H. C. Britt,[7] J. Chang,[3] C. Chasman,[1] Z. Chen,[1,‡] C.-Y. Chi,[4] Y. Y. Chu,[1] V. Cianciolo,[9,§] B. A. Cole,[4] H. J. Crawford,[2] J. B. Cumming,[1] R. Debbe,[1] J. C. Dunlop,[9] W. Eldredge,[3] J. Engelage,[2] S.-Y. Fung,[3] E. Garcia,[8] S. Gushue,[1] H. Hamagaki,[10] L. F. Hansen,[7] R. S. Hayano,[11] G. Heintzelman,[9] E. Judd,[2] J. Kang,[13] E.-J. Kim,[1,13] A. Kumagai,[12] K. Kurita,[12,‖] J.-H. Lee,[1] J. Luke,[7] Y. Miake,[12] A. Mignerey,[8] B. Moskowitz,[1] M. Moulson,[4] C. Muentz,[1,¶] S. Nagamiya,[5] M. N. Namboodiri,[7] C. A. Ogilvie,[9] J. Olness,[1] L. P. Remsberg,[1] H. Sako,[11,**] T. C. Sangster,[7] R. Seto,[3] J. Shea,[8] K. Shigaki,[11,††] R. Soltz,[9,‡‡] S. G. Steadman,[9] G. S. F. Stephans,[9] M. J. Tannenbaum,[1] J. H. Thomas,[7,*] S. Ueno-Hayashi,[12] F. Videbæk,[1] F. Wang,[4,*] Y. Wu,[4] H. Xiang,[3] G. H. Xu,[3] K. Yagi,[12] H. Yao,[9] W. A. Zajc,[4] and F. Zhu[1]

(E802 Collaboration)

[1]*Brookhaven National Laboratory, Upton, New York 11973*
[2]*University of California, Space Sciences Laboratory, Berkeley, California 94720*
[3]*University of California at Riverside, Riverside, California 92507*
[4]*Columbia University, New York 10027*
and Nevis Laboratories, Irvington, New York 10533
[5]*High Energy Accelerator Research Organization (KEK), Tsukuba, Ibaraki 305, Japan*
[6]*High Energy Accelerator Research Organization (KEK), Tanashi-branch, (Tanashi) Tokyo 188, Japan*
[7]*Lawrence Livermore National Laboratory, Livermore, California 94550*
[8]*University of Maryland, College Park, Maryland 20742*
[9]*Massachusetts Institute of Technology, Cambridge, Massachusets 02139*
[10]*Center for Nuclear Study, School of Science, University of Tokyo, Tanashi, Tokyo 188, Japan*
[11]*Department of Physics, University of Tokyo, Tokyo 113, Japan*
[12]*University of Tsukuba, Tsukuba, Ibaraki 305, Japan*
[13]*Yonsei University, Seoul 120-749, Korea*

(Received 23 March 1999; published 28 October 1999)

Proton and deuteron distributions from 11.6*A* GeV/*c* Au + Au collisions measured by the E802 Collaboration in experiment E-866 are presented. The invariant yield of protons and deuterons is studied as a function of the transverse mass for different cuts of rapidity and centrality. At low $m_t - m_0$ the proton and deuteron invariant spectra deviate from a single exponential shape. The average m_t as function of centrality and rapidity is used to explore the effect of collective transverse flow in the reaction. The ratio of the deuteron to squared proton yield as a function of transverse momentum, rapidity, and centrality is used to probe the coalescence model of deuteron production. This ratio is constant as a function of rapidity only for the most central cuts and decreases with the centrality for every rapidity cut. The ratio of the differential cross section of the deuteron to the squared differential cross section of the proton, for the most central cut, is not constant as a function of $m_t - m_0$. [S0556-2813(99)04911-0]

PACS number(s): 25.75.Dw, 25.75.Ld

I. INTRODUCTION

Heavy-ion collisions provide an opportunity to produce compression and heating of nuclear matter in a controlled environment. From the measured proton rapidity distributions of central Au + Au reactions at 11.6*A* GeV/*c* a significant increase of baryon stopping [1] was found as compared to earlier results using lighter systems [2], thus providing evidence for the formation of a larger interaction region and higher maximum density.

Among the several observables expected to result from the formation of dense nuclear matter is the manifestation of collective flow resulting from compression-induced pressure [3]. At around 10*A* GeV/*c*, azimuthally asymmetric particle correlations in the target rapidity region have been observed

*Present address: Lawrence Berkeley National Laboratory, Berkeley, CA 94720.

†Present address: Brookhaven National Laboratory, Upton, NY 11973.

‡Present address: Renaissance Technologies Corp., Stony Brook, NY 11790.

§Present address: Oak Ridge National Laboratory, Oak Ridge, TN 37831.

‖Present address: The Institute of Physical and Chemical Research (RIKEN), Saitama 351-01, Japan.

¶Present address: Goethe Universitaet, Institut fuer Kernphysik, Frankfurt, Germany.

**Present address: University of Tsukuba, Tsukuba, Ibaraki 305, Japan.

††Present address: High Energy Accel Res. Organization (KEK), Tsukuba, Ibaraki 305, Japan.

‡‡Present address: Lawrence Livermore National Laboratory, Livermore, CA 94550.

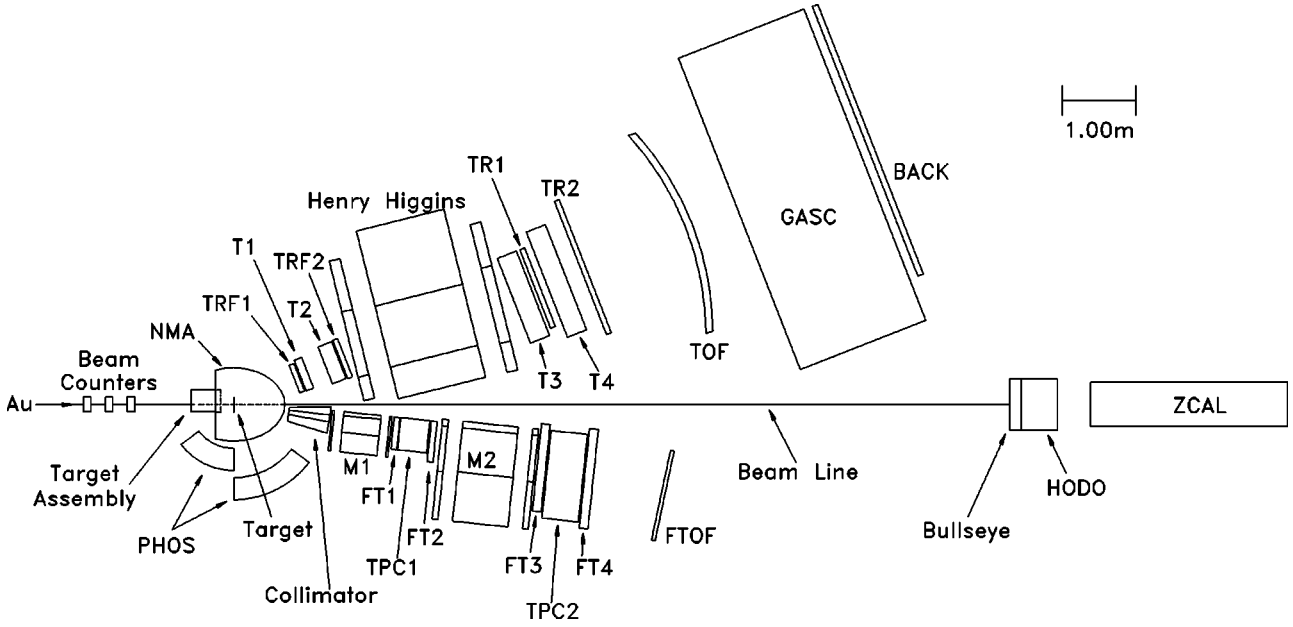

FIG. 1. The experimental layout of the E-866 in the Fall of 1994. Showed are the multiplicity array (NMA), the zero-degree calorimeter (ZCAL), the interaction trigger (Bullseye), the Henry Higgins spectrometer consisting of drift chambers (T1-T4), wire chambers (TRF1,2 and TR1,2), a time-of-flight wall (TOF), the gas-Cerenkov detector (GASC), and the back counter (BACK). The forward spectrometer consists of a sweeping magnet (M1), analyzing magnet (M2), drift chambers (FT1-4), two time projection chambers (TPC1,2) and a time-of-flight wall (FTOF). A scintillator array (PHOS) for particle spectra at back-angles and a hodoscope (HODO) of crossed XY slats complete the detector hardware.

[4], as well as ''bounce-off'' for protons [5]. Another predicted characteristic of collective flow is the shoulder-arm shape of the transverse momentum distributions and the increase with the mass of the slope parameters or average transverse mass ($\langle m_t \rangle$) for different particles [6]. Evidence of this has been observed in Au + Au at 11.6A GeV/c [1] and in Pb + Pb collisions at 158A GeV/c [7].

The nuclear matter formed in the interaction region is very hot and dense, but with time it expands and cools. At some point it is expected that the interactions among the particles cease and the nuclear matter is said to ''freeze-out.'' Deuterons are not elementary hadronic particles and

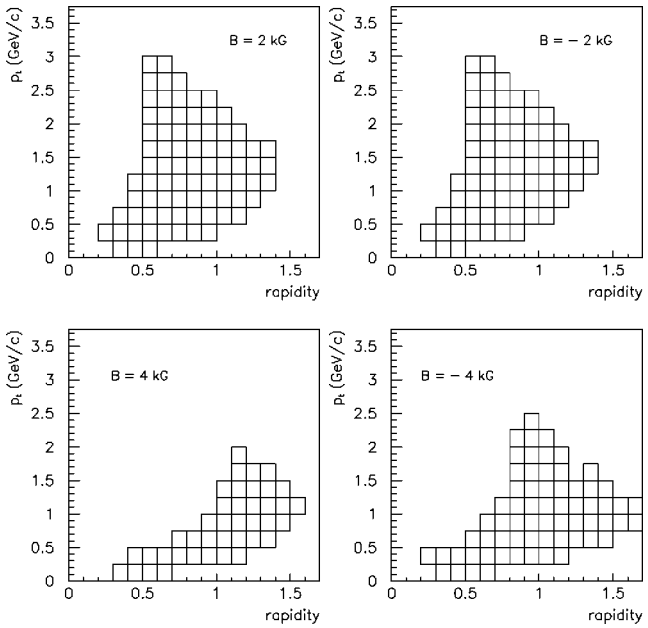

FIG. 2. Acceptance limits for protons, for the HH spectrometer at 14°, 19°, 24°, 29°, 34°, 39°, and 44°, for different magnet settings.

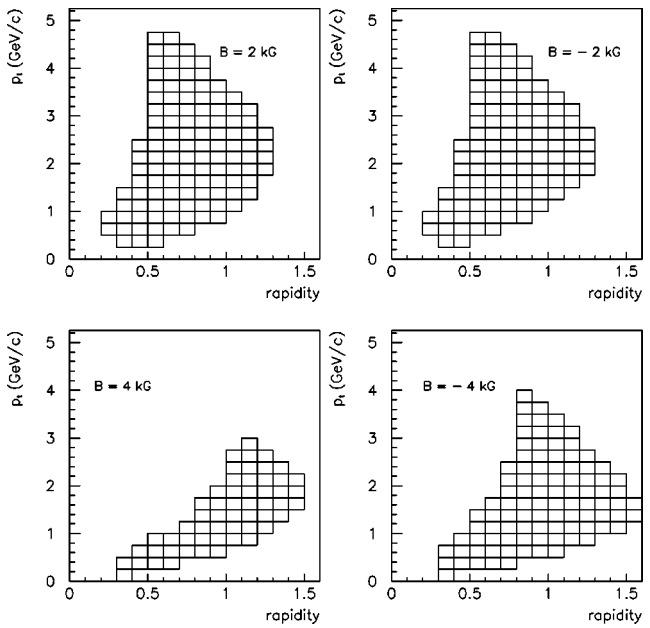

FIG. 3. Acceptance limits for deuterons, for the HH spectrometer at 14°, 19°, 24°, 29°, 34°, 39°, and 44°, for different magnet settings.

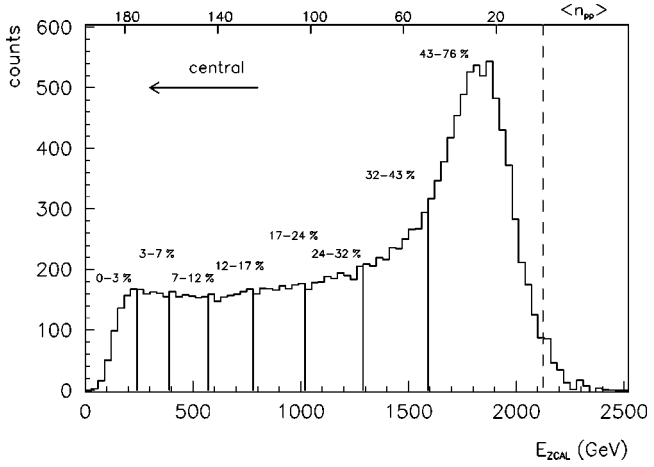

FIG. 4. The measured E_{ZCAL} distribution from interaction triggers. Target-out reactions have been subtracted. The centrality cuts used in the data analysis are illustrated by lines. The number of projectile participant nucleons, $\langle n_{pp}\rangle$, estimated from the E_{ZCAL} is indicated at the top of the figure. The beam-energy-centroid corresponding to $E_{\mathrm{ZCAL}}=2123.0$, is indicated with a dashed line.

because of their small binding energy (2.25 MeV), it is very probable that they will not survive repeated collisions [8,9]. Consequently it is likely that the observed deuterons are created from nucleons close to the freeze-out point. Thus composite particle production may provide information on the space-time structure of the freeze-out region.

Several models have been used to describe the production of light nuclear clusters or composites. In general, these models relate the invariant yields of light nuclei with mass A to the Ath power of the proton yields, and are commonly known as the coalescence models [10]. Specifically

$$E_A\frac{d^3n_A}{dp_A^3}=B_a\left(E_p\frac{d^3n_p}{dp_p^3}\right)^A, \quad p_A=Ap_p, \tag{1}$$

where B_a is the invariant coalescence factor and p_A is the cluster momentum, the assumption being that at these energies the unmeasured neutron distributions are identical to the measured proton distributions. At energies around $1A$ GeV/c, it was found that B_a was fairly independent of the centrality of the reaction and of the momentum and angle of emission of the cluster [11]. In the range of $10–15A$ GeV/c, it has been found that B_a is not a constant [12], and deviations from constant behavior have been addressed with more sophisticated models.

Some of these approaches treat the problem by considering energy-momentum conservation and the requirement of a third particle or a surrounding medium to form a deuteron from a nucleon pair [13,14]. Other models incorporate flow effects treating coalescence as an ''after-burner'' applied to the final nucleon density distribution provided by cascade calculations [6] or analytic hydrodynamic transport equations [15].

Using the relativistic quantum molecular dynamics model (RQMD) [16] and a cluster model based on the single-particle phase-space distributions at freeze-out, Mattiello *et al.* [17,6] showed that both the deviation from the exponential behavior (shoulder-arm shape) and the large bounce-off signal for clusters are directly related to the freeze-out geometry and flow correlations. As opposed to simple fireball and blast wave models that assume equal velocity and density profiles for all states, the freeze-out geometry and flow correlations result in smaller freeze-out radii and larger average transverse ''velocities,'' $\langle p_t\rangle/A$, for the clusters at midrapidities than for the protons. It is also shown that the collective flow enhances the deuteron yield, i.e., the probability of finding two nucleons close enough in the phase-space volume to produce a cluster.

If the coalescence model is applicable to the data, then the coalescence parameter B_a can be expressed in terms of an effective source volume, with equivalent radius R. The dependence of R on dynamical variables such as the transverse momentum can be used to probe how coalescence is affected by transverse flow.

In this paper, the proton and deuteron m_t-m_0 distributions from $11.6A$ GeV/c Au + Au reactions measured by the experiment E-866 at the Alternating Gradient Synchrotron (AGS) at Brookhaven National Laboratory in 1994 are presented. The rapidity distributions, dn/dy, and the average transverse mass $\langle m_t\rangle$ are extracted from the distributions. These parameters together with the ratio of deuteron yield to the square of the proton yield are studied as functions of the rapidity and centrality and this ratio is presented as a function of the transverse momentum for the most central cut. The implications of the data are analyzed in the context of the coalescence model and the possible effects of collective flow. In the following section a brief discussion of the ex-

TABLE I. Listing of the ranges of E_{ZCAL} values used as centrality cuts, and their equivalence in terms of the percentage of the cross section and the number of projectile participants.

E_{ZCAL} range (GeV)	CS range (mb)	% range	$\langle E_{\mathrm{ZCAL}}\rangle$ (GeV)	$\langle n_{pp}\rangle$
0–240	0–212	0–3	176.1	180
240–390	212–484	3–7	314.3	167
390–570	484–799	7–12	479.3	152
570–780	799–1174	12–17	676.3	134
780–1020	1174–1613	17–24	901.6	113
1020–1290	1613–2183	24–32	1158.5	89
1290–1590	2183–2976	32–43	1449.2	62
1590–3000	2976–5130	43–76	1832.6	27

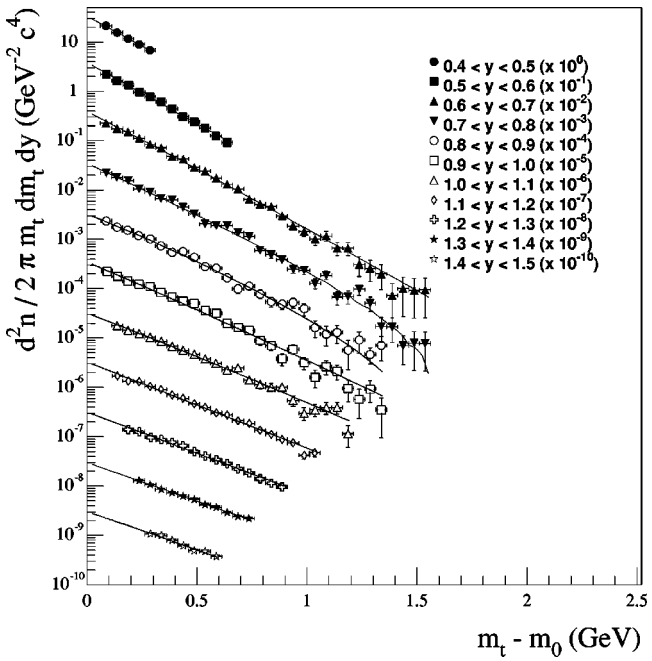

FIG. 5. Measured double differential yield for protons, in different rapidity intervals as a function of transverse kinetic energy $m_t - m_0$. This spectra is for the 0–3 % centrality cut. The lines are fits to Eq. (4) (see text). The error bars are only statistical; the systematic errors are discussed in the text.

periment is presented. Several aspects of the data analysis are considered in Sec. III. In Sec. IV the results are presented and a discussion follows in Sec. V. The last section presents the conclusions from this work.

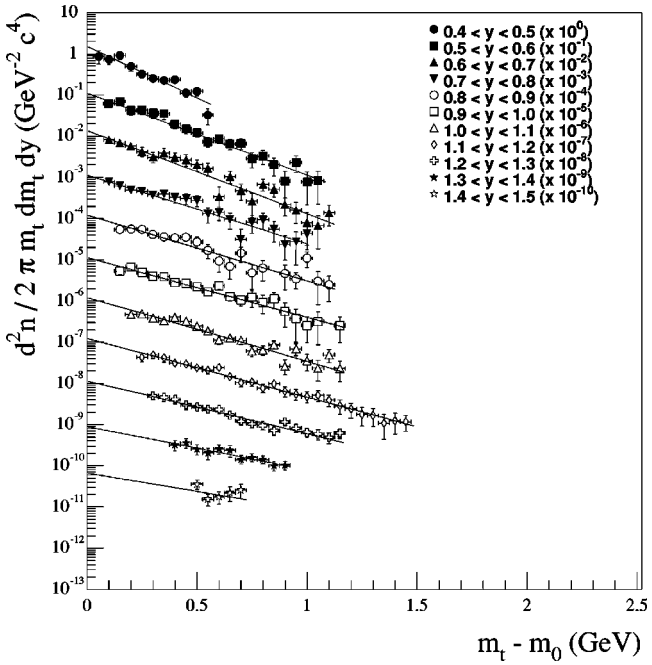

FIG. 6. Measured double differential yield for deuterons, in different rapidity intervals as a function of transverse kinetic energy $m_t - m_0$. These spectra are for the 0–3 % centrality cut. The lines are fits to Eq. (4) (see text). The error bars are only statistical; the systematic errors are discussed in the text.

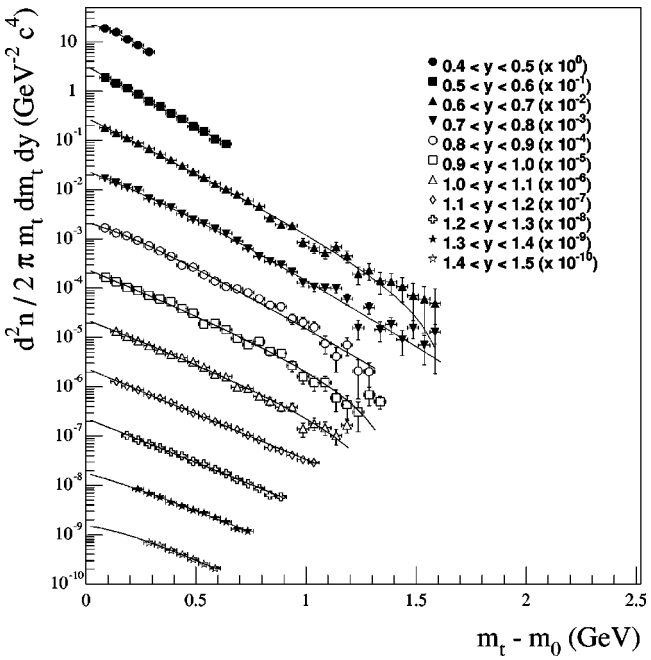

FIG. 7. Measured double differential yield for protons, in different rapidity intervals as a function of transverse kinetic energy $m_t - m_0$. These spectra are for the 12–17 % centrality cut. The lines are fits to Eq. (4) (see text). The error bars are only statistical; the systematic errors are discussed in the text.

II. THE EXPERIMENT

The present measurements were part of the study of 11.6*A* GeV/*c* Au + Au collisions in experiment E-866 at the AGS at Brookhaven National Laboratory by the E-802 collaboration. The E-866 apparatus consisted of three sets of detectors: for triggering, for identification and particle tracking, and for global characterization of the events. Experiment 866 had essentially the same setup as its predecessors E-859 and E-802, with some improvement to the tracking in front of the magnet, an additional forward spectrometer arm, and a new multiplicity array (NMA). The complete description of the Henry Higgins spectrometer and several aspects of E-802 can be found in Ref. [18], the elements of the experiment used for the measurements presented in this paper are briefly described in this section. A lay-out of the E-866 experiment is shown in Fig. 1.

Event triggering was defined by the ''beam counters'' BTOT and HOLE. These detectors were designed to determine good beam and timing for trigger logic and time-of-flight measurements. The BTOT was a quartz detector situated 2 m upstream of the target. HOLE was a scintillator detector with a 1 cm radius hole cut out of the middle, located 50 cm downstream of BTOT. In addition to these beam counters there was a quartz Cerenkov radiator (the ''bullseye'') [19] 10.6 m downstream from the target, which determined the charge of the forward-going spectator fragments.

The tracking and particle identification for this analysis were achieved using a rotatable 25 msr magnetic spectrometer (Henry Higgins), together with tracking detectors and the time-of-flight wall. The Henry Higgins spectrometer consisted of two drift chamber modules before (T1,T2) and two

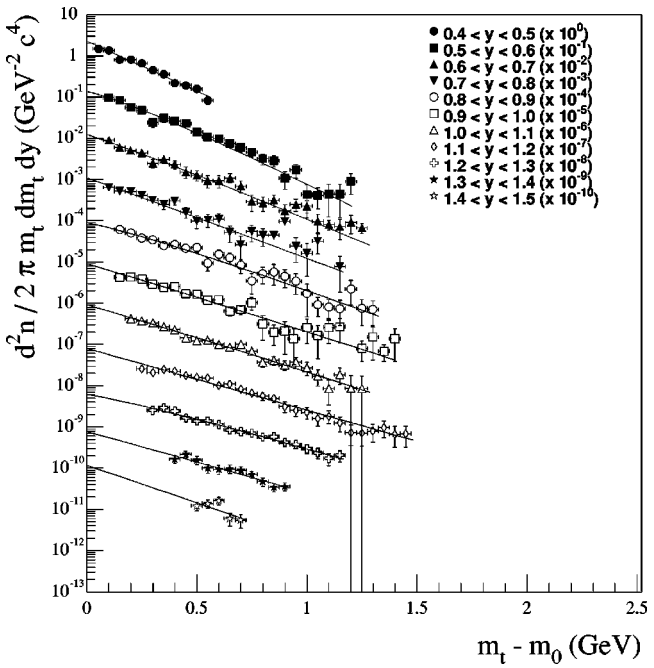

FIG. 8. Measured double differential yield for deuterons, in different rapidity intervals as a function of transverse kinetic energy $m_t - m_0$. These spectra are for the 12–17 % centrality cut. The lines are fits to Eq. (4) (see text). The error bars are only statistical; the systematic errors are discussed in the text.

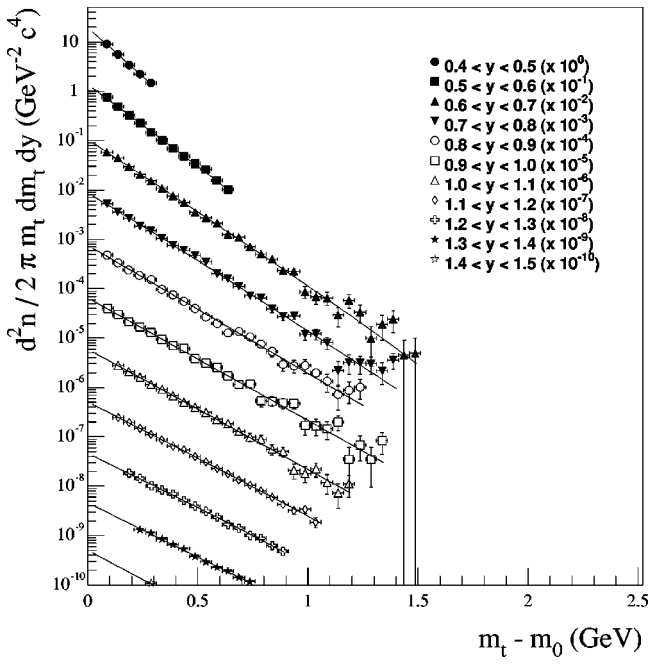

FIG. 9. Measured double differential yield for protons, in different rapidity intervals as a function of transverse kinetic energy $m_t - m_0$. These spectra are for the 43–76 % centrality cut. The lines are fits to Eq. (4) (see text). The error bars are only statistical; the systematic errors are discussed in the text.

after (T3,T4) the magnet. The single track resolution of the chambers was 150 μm and for two tracks, about 2 mm. The wire tracking chambers TRF1 and TRF2 were built to help the spectrometer handle the high multiplicity events. Each chamber consisted of four planes of wires, one each in the horizontal, vertical, and the two diagonal directions. Finally the time-of-flight wall (TOF) [20], consisting of 160 plastic scintillators placed 6.5 m from the target, with a timing resolution of about 130 ps (1σ), was used for particle identification. The platform carrying the magnet, tracking, and particle identification detectors can swing the spectrometer from a most forward angle of 14° to a most backward angle of 44°.

The centrality selection for the spectra was made using the zero degree calorimeter (ZCAL) [21], which measured the energy remaining in the projectile fragments traveling forward, and which subtended an angle of 1.5° from the beam axis.

Several hardware triggers were implemented in E-866. The valid beam trigger (BEAM), was logically defined by $BEAM = \overline{PRE} \cap BTOT \cap HOLE$, where PRE is a 0.5 μs pile-up rejection criterion; the interaction trigger, $INT = BEAM \cap \overline{BE}$, where BE means a valid bullseye interaction. and the level zero trigger, $LVL0 = (BEAM/n \cup INT) \cap \overline{TBUSY}$, with $n = 200$ and TBUSY a busy-processing signal. For the measurements presented in this paper the SPEC trigger was used. It was a minimum bias trigger which required a valid beam, an interaction and a hit in at least one of the TOF slats and one of the TRF1 wires $SPEC = LVL0 \cap TOF1 \cap TR1$. The SPEC-triggered data are not biased against any particle species and also represent a minimum bias trigger.

The thickness of the Au target was 1.5% of an Au interaction length, or 975 mg/cm^2 (Gold nuclei at 11.6A GeV/c

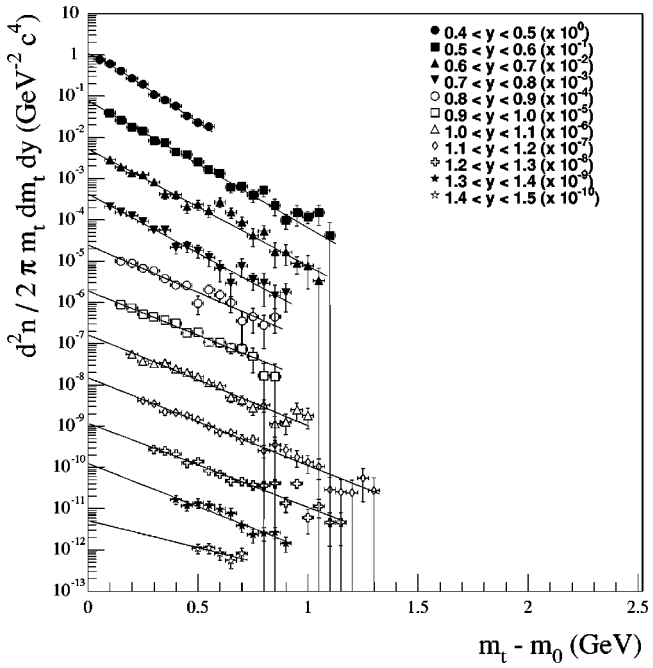

FIG. 10. Measured double differential yield for deuterons, in different rapidity intervals as a function of transverse kinetic energy $m_t - m_0$. These spectra are for the 43–76 % centrality cut. The lines are fits to Eq. (4) (see text). The error bars are only statistical; the systematic errors are discussed in the text.

TABLE II. The dn/dy and $\langle m_t \rangle$ distributions for protons. Each centrality cut is defined in Table I. The errors cited are statistical only.

y	dn/dy	$\langle m_t \rangle$ (GeV)	χ^2/d.o.f.
	0–3 % centrality		
0.45±0.05	41.7±1.1	1.140±0.013	0.31/5
0.55±0.05	47.2±1.2	1.140±0.005	8.19/12
0.65±0.05	51.6±1.2	1.152±0.002	27.60/30
0.75±0.05	51.3±1.2	1.169±0.003	39.62/30
0.85±0.05	53.3±1.1	1.182±0.007	26.21/26
0.95±0.05	56.4±1.0	1.198±0.002	44.15/26
1.05±0.05	58.2±1.0	1.226±0.002	23.61/22
1.15±0.05	60.5±1.0	1.239±0.005	28.88/19
1.25±0.05	61.6±1.2	1.255±0.007	18.37/15
1.35±0.05	63.2±1.7	1.278±0.013	2.70/11
	3–7 % centrality		
0.45±0.05	42.6±1.0	1.126±0.011	1.26/5
0.55±0.05	47.6±1.1	1.144±0.005	6.32/12
0.65±0.05	50.3±1.1	1.154±0.002	37.36/30
0.75±0.05	50.6±1.1	1.173±0.003	19.85/28
0.85±0.05	52.4±1.0	1.185±0.004	29.07/26
0.95±0.05	53.0±0.9	1.184±0.005	30.25/26
1.05±0.05	55.7±0.9	1.212±0.002	25.15/22
1.15±0.05	56.2±0.9	1.230±0.005	19.68/19
1.25±0.05	55.3±1.0	1.250±0.002	23.81/15
1.35±0.05	55.8±1.3	1.285±0.013	4.43/11
	7–12 % centrality		
0.45±0.05	41.5±1.0	1.125±0.013	3.16/5
0.55±0.05	44.6±1.0	1.145±0.003	12.36/12
0.65±0.05	43.9±0.7	1.158±0.002	31.32/32
0.75±0.05	45.5±0.8	1.172±0.003	22.27/31
0.85±0.05	46.2±0.8	1.174±0.002	24.47/27
0.95±0.05	47.7±0.8	1.200±0.005	24.65/25
1.05±0.05	47.8±0.8	1.207±0.002	29.50/21
1.15±0.05	49.0±0.8	1.224±0.005	20.35/19
1.25±0.05	48.1±0.9	1.233±0.002	16.01/15
1.35±0.05	48.7±4.2	1.245±0.011	5.91/11
	12–17 % centrality		
0.45±0.05	35.1±3.5	1.121±0.010	5.23/5
0.55±0.05	39.7±0.9	1.140±0.004	4.22/12
0.65±0.05	38.9±0.7	1.153±0.002	37.45/31
0.75±0.05	38.8±0.8	1.174±0.005	29.22/31
0.85±0.05	38.6±0.8	1.180±0.005	23.29/25
0.95±0.05	40.0±0.7	1.178±0.004	26.96/26
1.05±0.05	39.3±0.9	1.183±0.009	22.16/22
1.15±0.05	41.1±0.7	1.220±0.005	9.21/19
1.25±0.05	41.4±0.8	1.231±0.006	10.30/15
1.35±0.05	38.5±3.4	1.249±0.012	6.85/11
	17–24 % centrality		
0.45±0.05	36.6±0.9	1.107±0.010	1.12/5
0.55±0.05	34.8±1.2	1.122±0.006	4.84/12
0.65±0.05	34.6±0.6	1.145±0.002	29.25/31
0.75±0.05	34.8±0.7	1.156±0.002	34.39/30
0.85±0.05	34.3±0.6	1.164±0.004	24.66/27
0.95±0.05	33.8±0.6	1.178±0.004	13.67/26
1.05±0.05	33.3±0.7	1.190±0.007	20.92/21
1.15±0.05	34.5±0.64	1.207±0.004	12.85/19
1.25±0.05	34.3±0.7	1.216±0.006	8.92/15
1.35±0.05	32.8±4.2	1.237±0.024	2.17/11
	24–32 % centrality		
0.45±0.05	30.2±2.2	1.089±0.003	1.34/5
0.55±0.05	29.1±1.0	1.119±0.007	5.65/12
0.65±0.05	27.6±0.5	1.136±0.002	32.65/31
0.75±0.05	27.2±0.5	1.146±0.003	17.61/28
0.85±0.05	26.6±0.5	1.159±0.004	19.21/26
0.95±0.05	25.9±0.4	1.171±0.004	17.53/26
1.05±0.05	25.9±0.4	1.181±0.004	18.31/22
1.15±0.05	25.3±0.4	1.199±0.004	12.25/19
1.25±0.05	25.4±0.5	1.208±0.005	14.35/15
1.35±0.05	25.8±1.9	1.213±0.011	5.86/11
	32–43 % centrality		
0.45±0.05	24.7±0.7	1.080±0.007	0.30/5
0.55±0.05	22.5±0.5	1.110±0.003	8.73/12
0.65±0.05	20.2±0.3	1.128±0.002	31.25/32
0.75±0.05	19.5±0.4	1.137±0.003	14.70/27
0.85±0.05	19.2±0.3	1.145±0.003	24.47/29
0.95±0.05	18.3±0.3	1.149±0.004	24.60/26
1.05±0.05	17.2±0.4	1.166±0.005	21.97/22
1.15±0.05	16.9±0.4	1.181±0.004	11.64/19
1.25±0.05	16.4±0.7	1.194±0.006	7.31/15
1.35±0.05	16.6±0.5	1.196±0.007	4.82/11
	43–76 % centrality		
0.45±0.05	14.0±0.4	1.059±0.006	2.59/5
0.55±0.05	12.1±0.3	1.085±0.003	11.35/12
0.65±0.05	10.6±0.2	1.105±0.001	26.41/29
0.75±0.05	9.6±0.2	1.118±0.002	31.98/27
0.85±0.05	8.8±0.2	1.131±0.003	25.40/24
0.95±0.05	8.0±0.1	1.141±0.004	22.72/26
1.05±0.05	7.4±0.2	1.146±0.004	10.10/22
1.15±0.05	6.9±0.2	1.158±0.003	5.93/19
1.25±0.05	6.5±0.2	1.162±0.006	9.98/15
1.35±0.05	6.5±0.4	1.172±0.006	8.59/11

TABLE III. The dn/dy and $\langle m_t \rangle$ distributions for deuterons. Each centrality cut defined in Table I. The errors cited are statistical only.

y	dn/dy	$\langle m_t \rangle$ (GeV)	χ^2/d.o.f.	y	dn/dy	$\langle m_t \rangle$ (GeV)	χ^2/d.o.f.
	0–3 % centrality				17–24 % centrality		
0.45±0.05	3.4±0.3	2.064±0.023	19.52/11	0.45±0.05	4.6±0.3	2.076±0.011	6.30/11
0.55±0.05	3.2±0.2	2.117±0.012	14.67/20	0.55±0.05	3.9±0.2	2.084±0.009	32.45/23
0.65±0.05	3.9±0.2	2.114±0.015	21.62/21	0.65±0.05	3.4±0.1	2.106±0.008	15.52/26
0.75±0.05	4.0±0.2	2.167±0.022	13.90/19	0.75±0.05	3.3±0.2	2.140±0.017	5.68/20
0.85±0.05	4.5±0.2	2.182±0.022	23.31/19	0.85±0.05	2.9±0.2	2.143±0.034	21.32/24
0.95±0.05	4.6±0.2	2.217±0.025	13.34/20	0.95±0.05	2.7±0.1	2.155±0.015	22.70/22
1.05±0.05	4.6±0.3	2.191±0.018	31.14/20	1.05±0.05	2.8±0.1	2.172±0.014	14.92/24
1.15±0.05	5.1±0.3	2.222±0.018	12.55/25	1.15±0.05	2.7±0.2	2.168±0.012	21.11/25
1.25±0.05	5.4±0.5	2.265±0.027	14.04/18	1.25±0.05	2.7±0.2	2.225±0.020	20.39/18
1.35±0.05	5.3±0.6	2.347±0.053	3.32/11	1.35±0.05	2.7±0.3	2.193±0.032	11.54/11
	3–7 % centrality				24–32 % centrality		
0.45±0.05	4.2±0.4	2.087±0.018	8.73/11	0.45±0.05	4.1±0.2	2.070±0.010	7.29/11
0.55±0.05	3.8±0.2	2.121±0.009	15.13/21	0.55±0.05	3.4±0.2	2.076±0.009	23.59/23
0.65±0.05	4.0±0.2	2.135±0.008	20.61/26	0.65±0.05	2.8±0.1	2.098±0.011	22.42/22
0.75±0.05	4.2±0.2	2.157±0.017	10.32/22	0.75±0.05	2.4±0.1	2.129±0.022	16.42/20
0.85±0.05	4.6±0.2	2.157±0.016	18.15/26	0.85±0.05	2.2±0.2	2.110±0.043	16.13/19
0.95±0.05	4.4±0.2	2.210±0.021	12.24/24	0.95±0.05	2.1±0.1	2.133±0.015	10.86/18
1.05±0.05	4.4±0.6	2.183±0.040	15.70/24	1.05±0.05	1.8±0.1	2.183±0.015	10.87/21
1.15±0.05	4.7±0.3	2.204±0.015	17.19/25	1.15±0.05	1.9±0.1	2.153±0.013	27.58/25
1.25±0.05	4.4±0.3	2.246±0.027	14.27/18	1.25±0.05	2.0±0.2	2.150±0.014	33.31/18
1.35±0.05	4.6±0.7	2.227±0.041	15.70/11	1.35±0.05	2.0±0.3	2.150±0.030	10.56/11
	7–12 % centrality				32–43 % centrality		
0.45±0.05	4.1±0.2	2.088±0.016	6.11/11	0.45±0.05	3.5±0.3	2.031±0.020	7.44/11
0.55±0.05	4.1±0.2	2.107±0.008	19.71/25	0.55±0.05	2.8±0.1	2.053±0.007	23.25/23
0.65±0.05	4.0±0.2	2.081±0.022	25.42/25	0.65±0.05	2.3±0.1	2.077±0.010	11.89/22
0.75±0.05	3.8±0.2	2.128±0.014	22.90/23	0.75±0.05	1.8±0.1	2.095±0.013	16.19/21
0.85±0.05	4.0±0.2	2.156±0.017	14.73/22	0.85±0.05	1.5±0.2	2.089±0.011	17.75/19
0.95±0.05	4.0±0.2	2.196±0.018	11.87/25	0.95±0.05	1.5±0.1	2.113±0.016	18.95/19
1.05±0.05	3.8±0.2	2.213±0.017	20.28/23	1.05±0.05	1.5±0.2	2.111±0.009	15.64/20
1.15±0.05	4.2±0.2	2.190±0.013	32.47/25	1.15±0.05	1.2±0.1	2.139±0.013	17.00/24
1.25±0.05	4.0±0.3	2.221±0.019	14.89/18	1.25±0.05	1.3±0.1	2.123±0.014	12.76/18
1.34±0.05	4.1±0.5	2.270±0.039	11.60/11	1.35±0.05	1.0±0.2	2.138±0.032	5.17/11
	12–17 % centrality				43–76 % centrality		
0.45±0.05	5.3±0.3	2.070±0.011	10.13/11	0.45±0.05	2.0±0.14	2.013±0.007	6.21/11
0.55±0.05	4.1±0.2	2.102±0.010	25.36/23	0.55±0.05	1.4±0.06	2.026±0.004	18.85/21
0.65±0.05	3.7±0.2	2.110±0.011	23.60/24	0.65±0.05	1.0±0.04	2.041±0.009	23.19/20
0.75±0.05	3.3±0.1	2.122±0.016	22.84/21	0.75±0.05	0.83±0.03	2.037±0.008	16.30/17
0.85±0.05	3.6±0.3	2.165±0.018	14.46/24	0.85±0.05	0.60±0.03	2.082±0.013	12.85/15
0.95±0.05	3.3±0.1	2.169±0.017	27.09/25	0.95±0.05	0.50±0.02	2.098±0.013	8.73/15
1.05±0.05	3.4±0.1	2.170±0.019	17.74/22	1.05±0.05	0.42±0.03	2.092±0.014	19.91/17
1.15±0.05	3.2±0.2	2.204±0.014	23.52/25	1.15±0.05	0.40±0.03	2.100±0.011	11.04/22
1.25±0.05	3.0±0.6	2.236±0.044	6.30/18	1.25±0.05	0.33±0.04	2.111±0.020	20.14/18
1.35±0.05	3.1±0.4	2.205±0.037	7.55/11	1.35±0.05	0.34±0.07	2.103±0.027	7.80/11

have a total inelastic cross section of 6.78 barns [22]). The intensity of the Au^{+79} beam was typically 1×10^5 particles per spill, with each spill about 1 s long every 4 s. The size of the beam was typically 2 mm vertically and 4 mm horizontally. Target-out runs were performed to determine the background contributions. The target out contributions to the spectra were very small and affected only the cross-section normalization.

III. DATA ANALYSIS

The acceptance limits of the Henry Higgins (HH) arm for protons and deuterons is shown in Figs. 2 and 3, respec-

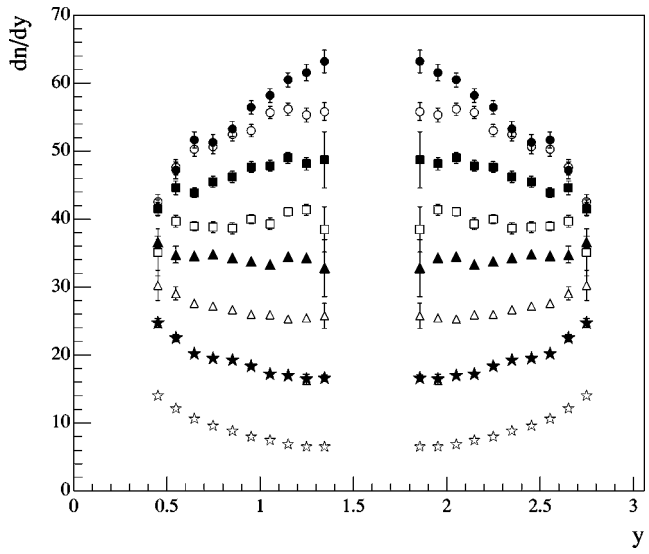

FIG. 11. The dn/dy distributions of protons for different centrality cuts (as listed in Table I). The circles are for the 0–3 % centrality cut, the open circles are for the 3–7 % centrality cut, the squares are for the 7–12 % centrality cut, the open squares are for the 12–17 % centrality cut, the triangles are for the 17–24 % centrality cut, the open triangles are for the 24–32 % centrality cut, the stars are for the 32–43 % centrality cut, and the open stars are for the 43–76 % centrality cut. The data points are reflected about midrapidity. The vertical error bars are statistical only; the systematic errors are discussed in the text.

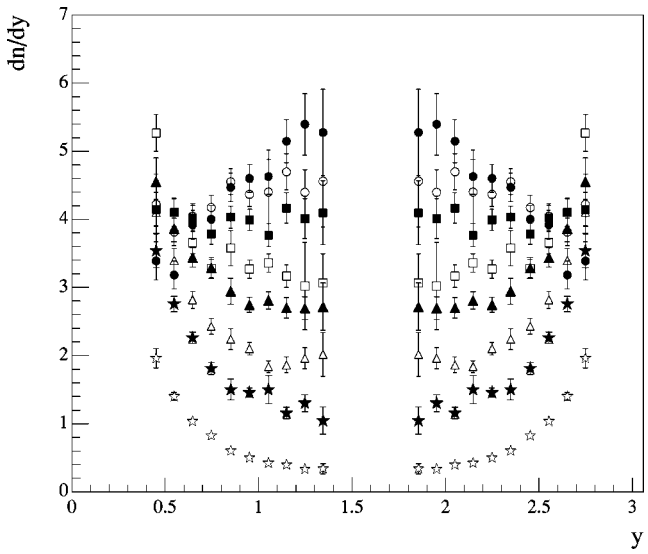

FIG. 12. The dn/dy distributions of deuterons for different centrality cuts (as listed in Table I). The circles are for the 0–3 % centrality cut, the open circles are for the 3–7 % centrality cut, the squares are for the 7–12 % centrality cut, the open squares are for the 12–17 % centrality cut, the triangles are for the 17–24 % centrality cut, the open triangles are for the 24–32 % centrality cut, the stars are for the 32–43 % centrality cut, and the open stars are for the 43–76 % centrality cut. The data points are reflected about midrapidity. The vertical error bars are statistical only; the systematic errors are discussed in the text.

tively. The acceptance is constrained by the geometry of the HH (spectrometer angle and magnet setting) and the tracking inefficiency (at low p_t). It is shown versus rapidity and transverse momentum and for different magnet settings in Figs. 2 and 3 for the HH spectrometer angle settings used in the present study, 14°, 19°, 24°, 34°, 39°, and 44°. The rapidity between the target and projectile is 3.2, so that the midrapidity, y_{nn}, is 1.6.

The yield of protons and deuterons was corrected to account for the efficiency for detecting particles in the spectrometer. The inefficiencies arise from two effects: inefficiencies due to single track loses, and those due to high occupancy loses. The single track inefficiencies are due to detector effects, multiple scattering, track code failures, and hadronic interactions. Monte Carlo simulations based on GEANT [23] were performed to estimate the particle loss due to these effects. The single track inefficiencies were significant for protons and deuterons at the limits of the momentum acceptance of the detector, that is at very high or low particle momentum. In order to avoid a correction factor larger than 15%, momentum limits were set at $0.3\ \mathrm{GeV}/c \leqslant p \leqslant 3.5\ \mathrm{GeV}/c$ for protons and $0.6\ \mathrm{GeV}/c \leqslant p \leqslant 5.7\ \mathrm{GeV}/c$ for the deuterons.

The main causes for the inefficiencies due to high occupancy are failures of the track finding algorithm and uncertainties of hit position from hit blocking in the TOF. The loss of tracks due to hit blocking in Au + Au events was studied using a track insertion technique [22]. In this method two events are merged, one of them chosen with relatively clean tracks. The merged events are then reconstructed and compared to the results for each event separately. This method allows a large statistics study of high multiplicity effects.

It should be noted that since the magnetic rigidity of the deuterons and the α particles is the same, an α particle with twice the momentum of a deuteron will have the same trajectory through the magnet and the same time of flight, that is, it is not possible to distinguish between α particles and deuterons in this experimental arrangement. Thus the spectra of the deuterons may have some contamination of α particles. At AGS energies however, the yield ratio of α's to deuterons has been found to be very small $\alpha/d \simeq 10^{-3}$ [12], consistent with the E-866 observation of tritons at mid rapidity, and for deuterons and tritons at target rapidity [24]. These results are also consistent with theoretical estimations of cluster production [6]. Therefore, the effect of the α contamination on the deuteron distributions can be neglected.

The event centrality selection for the invariant spectra was made using the ZCAL. The energy deposited into the zero degree calorimeter, E_{ZCAL}, for interaction events after target-out subtraction, is shown in Fig. 4. The boundaries for the centrality cuts used in this analysis are shown, together with the estimated number of projectile participants, $\langle n_{pp} \rangle$. Since the energy in this detector is predominantly from projectile spectators, the number of projectile participants is empirically estimated by

$$\langle n_{pp} \rangle = 197.0 \left(1 - \frac{E_{\mathrm{ZCAL}}}{2123} \right), \tag{2}$$

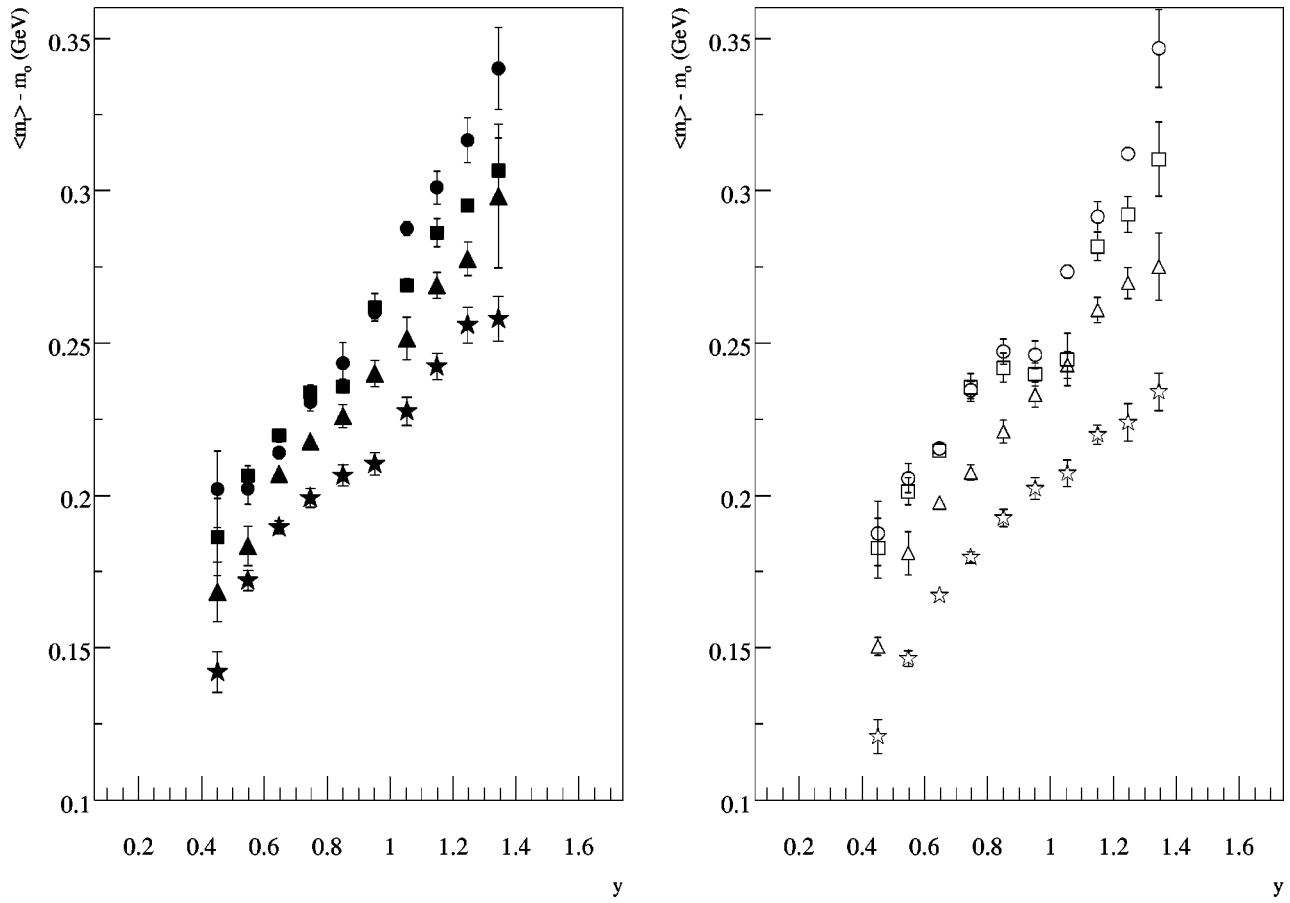

FIG. 13. The average transverse mass $\langle m_t \rangle - m_0$ as a function of the rapidity for protons, for the different centrality cuts (as listed in Table I). The circles are for the 0–3 % centrality cut, the open circles are for the 3–7 % centrality cut, the squares are for the 7–12 % centrality cut, the open squares are for the 12–17 % centrality cut, the triangles are for the 17–24 % centrality cut, the open triangles are for the 24–32 % centrality cut, the stars are for the 32–43 % centrality cut, and the open stars are for the 43–76 % centrality cut. The vertical error bars are statistical only; the systematic errors are discussed in the text.

where E_{ZCAL} is the energy measured in GeV in the ZCAL and 2123 GeV is the approximate energy of the beam. It has been estimated that the systematic errors in evaluating $\langle n_{pp} \rangle$ are about 8% for midcentral to central collisions [21]. For the most peripheral events the calorimeter had a nonlinear response, that leads to an uncertainty of up to eight in the value of $\langle n_{pp} \rangle$, or of about 25%. Table I lists of the ranges of ZCAL values used as centrality cuts, the corresponding range of the inelastic cross section in mb, and the percentage in reference to the total inelastic cross section of 6.78 barns. The last two columns are the average value of ZCAL for the events in that range and $\langle n_{pp} \rangle$ calculated with Eq. (2). The percentage column lists the range of the total inelastic cross section for the cut, with 0% corresponding to impact parameter zero.

The overall systematic error is estimated to be of the order of 10% in the measurement of the differential yield. However, in the figures shown in the next section, only statistical errors are displayed.

IV. RESULTS

The azimuthally averaged invariant double differential yield is given by

$$\frac{1}{2\pi} \frac{d^2n}{m_t dm_t dy}, \tag{3}$$

where y is the rapidity, $m_t = \sqrt{p_t^2 + m_0^2}$, with m_0 being the rest mass of the particle and $p_t = p \sin\theta$ is the transverse momentum, with θ being the polar angle. Figures 5–10 show the measured invariant double differential yield for protons and deuterons as a function of $m_t - m_0$ at different rapidity intervals, and three centrality cuts. The deuteron spectra are harder than the proton spectra, especially for the most central cut. Both the proton and deuteron spectra tend to deviate from an exponential shape at low $m_t - m_0$. Again, the deviation is larger for the deuteron spectra, and for the most central cut. The proton spectra cannot be described with a single exponential [1]. The same is observed for the deuteron spectra. The differential yields were fit instead to the more general function,

$$\frac{d^2n}{2\pi m_t dm_t dy} = A_1 m_t \exp\left(\frac{-(m_t - m_0)}{T_1}\right) + A_2 \exp\left(\frac{-(m_t - m_0)}{T_2}\right), \tag{4}$$

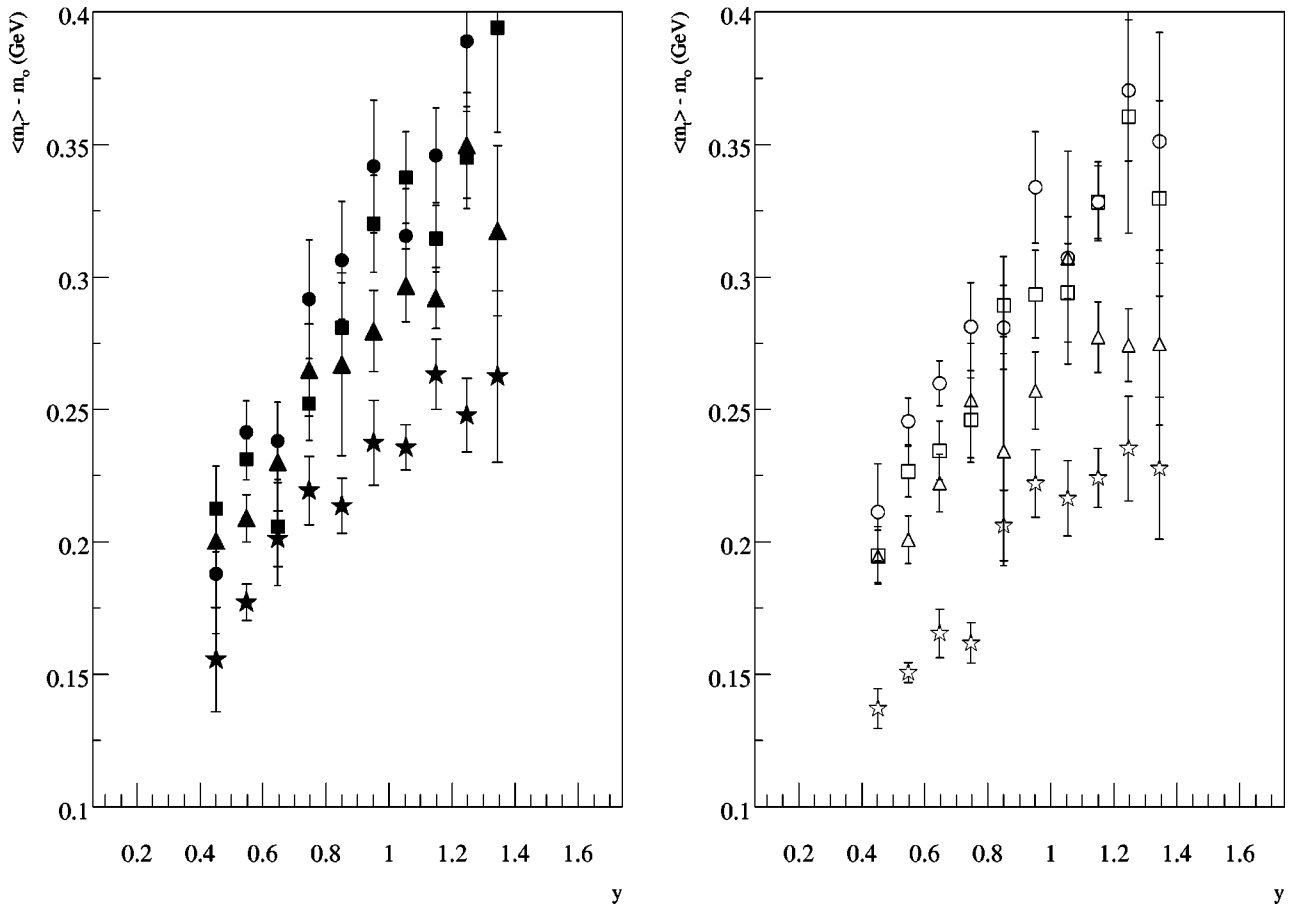

FIG. 14. The average transverse mass $\langle m_t \rangle - m_0$ as a function of the rapidity for deuterons, for the different centrality cuts. (As listed in Table I.) The circles are for the 0–3 % centrality cut, the open circles are for the 3–7 % centrality cut, the squares are for the 7–12 % centrality cut, the open squares are for the 12–17 % centrality cut, the triangles are for the 17–24 % centrality cut, the open triangles are for the 24–32 % centrality cut, the stars are for the 32–43 % centrality cut, and the open stars are for the 43–76 % centrality cut. The vertical error bars are statistical only; the systematic errors are discussed in the text.

where A_i and T_i are parameters. Note that A_1 and A_2 can be written as a function of dn/dy and average transverse mass $\langle m_t \rangle$, by integrating Eq. (4),

$$\frac{dn}{dy} = \int_{m_0}^{\infty} dm_t 2\pi m_t \frac{d^2n}{2\pi m_t dm_t dy}, \tag{5}$$

$$\langle m_t \rangle = \int_{m_0}^{\infty} 2\pi m_t^2 \frac{d^2n}{2\pi m_t dm_t dy} \Big/ \int_{m_0}^{\infty} 2\pi m_t \frac{d^2n}{2\pi m_t dm_t dy}. \tag{6}$$

Broad physical limits were set on the $\langle m_t \rangle$ for the minimization process. The errors on the fit parameters dn/dy, $\langle m_t \rangle$, T_1, and T_2 are the diagonal terms of the error matrix given by MINUIT [25], in which the errors are obtained from the variation of the χ^2 around the minimum. For the rapidity bin $1.4 < y < 1.5$ of the deuteron spectra and the bin $0.4 < y < 0.5$ of the proton spectra, the data points were insufficient to fit the distributions to four parameters, for these spectra a Boltzmann function was used to to calculate the dn/dy and $\langle m_t \rangle$ [$A_2 = 0$ in Eq. (4)].

The dn/dy and $\langle m_t \rangle$ parameters were observed to be uncorrelated. Other parametrizations yielded similar results for the values of dn/dy and $\langle m_t \rangle$, within the systematic error. It is estimated that the systematic error in the estimation of dn/dy is about $\pm(10-15)\%$, and in $\langle m_t \rangle$ of $\pm 10\%$. However, the error bars shown in the figures are only from the statistical errors. The complete set of dn/dy and $\langle m_t \rangle$ values for all the centrality cuts are tabulated in Tables II and III.

Figure 11 shows the distributions of particle yield, dn/dy, as a function of the rapidity, y, for protons. The different centrality groups (Table I) are indicated by different symbols, and the data points are reflected about midrapidity. For the peripheral cut for the protons dn/dy is peaked towards target rapidity and resembles the distributions for inelastic p-p data [26] with a small yield at midrapidity ($y \simeq 1.6$). As the centrality increases the distributions become flatter. The dn/dy distribution for the 12–17 % cut already peaks at midrapidities. Finally, for the most central cut the data exhibit a clear maximum at midrapidity. As discussed in [1], this provides strong evidence for a large amount of stopping, and the consequent expectation of high baryon density.

The deuteron dn/dy distributions are shown in Fig. 12. The different centrality groups (Table I) are again indicated by different symbols and the data points are reflected around midrapidity. In general, the deuteron rapidity distributions

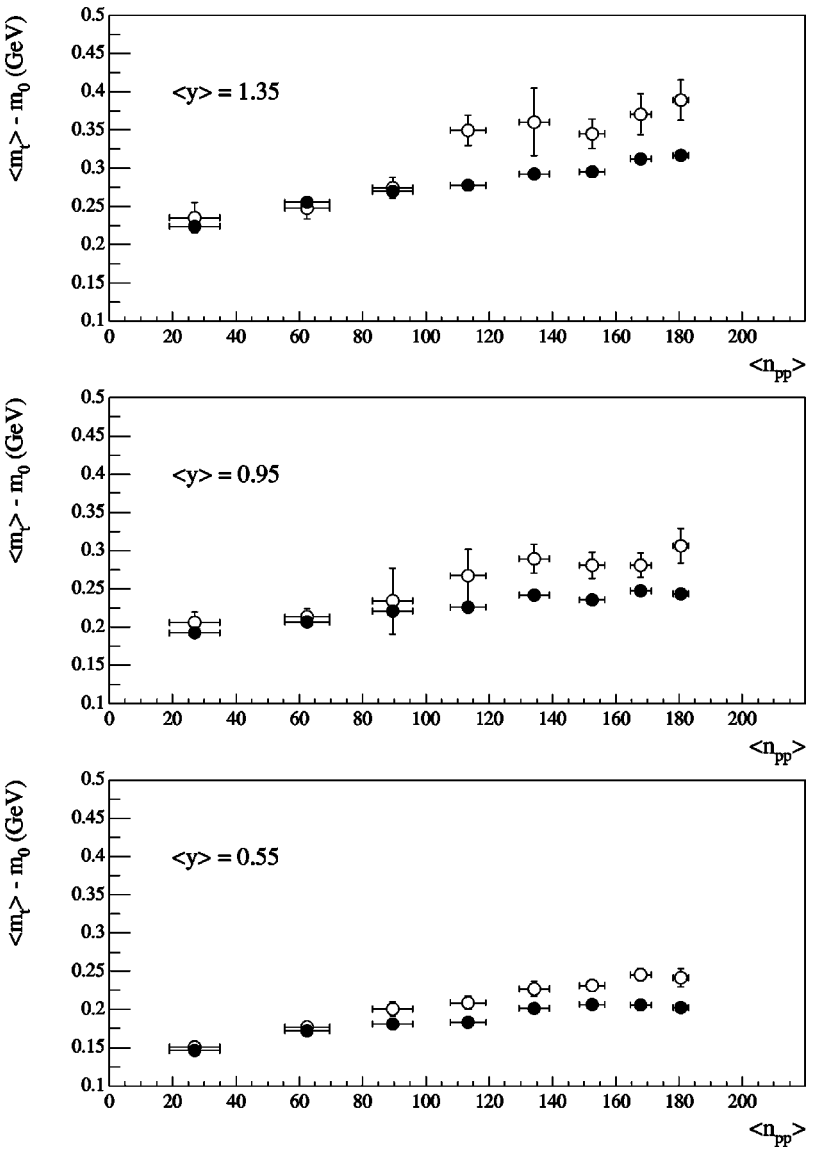

FIG. 15. Difference of averaged transverse mass $\langle m_t \rangle - m_0$ of protons (circles) and deuterons (open circles) as a function of the number of projectile participants $\langle n_{pp} \rangle$ for three rapidity bins, $y = 0.55$, $y = 0.95$, and $y = 1.35$. The error bars are only statistical; the systematic errors are discussed in the text.

follow the trend for the the protons. There is, however, a distinctive difference between the spectra: the change of shape of the distributions from concave to convex occurs at more central bins for the deuterons than for the protons. Particularly for the peripheral collisions, the rapidity distributions of the protons appear to be flatter than those of the deuterons.

The mean transverse mass minus the rest mass, $\langle m_t \rangle - m_0$, is shown as function of the rapidity in Figs. 13 and 14 for protons and deuterons, respectively. The different centrality groups (cited in Table I) are indicated by different symbols. For the protons and the deuterons, the $\langle m_t \rangle - m_0$ increases with rapidity for all centrality cuts, also for a given rapidity bin the $\langle m_t \rangle - m_0$ increases steadily as a function of centrality. The increase in the transverse mass of the deuterons as function of rapidity is more pronounced than the increase in the protons. This is shown in Fig. 15 where the $\langle m_t \rangle - m_0$ of the deuterons and protons is plotted as a function of the number of participant nucleons ($\langle n_{pp} \rangle$) for three rapidity bins. The difference between the transverse mass of the deuterons and the protons is larger for the midrapidity regions and more central bins (greater $\langle n_{pp} \rangle$).

V. DISCUSSION

A heavy-ion collision results in the production of hot and dense nuclear matter. As the matter cools and/or expands, the interactions between particles within this volume are less frequent and occur at low relative momentum. In the coalescence picture, sufficiently close nucleons at relatively close momentum can fuse to form light nuclei [10]. Within this model, it is expected that the invariant cross section for the production of a deuteron is proportional to the square of the proton phase-space density [Eq. (1)].

In a simple thermodynamical model, B_a of Eq. (1) is inversely related to the source volume (V_{source}) [27], depending very weakly on the transverse momentum, and independent of y [11]. The independence of B_a as a function of transverse momentum and rapidity is regarded as scaling behavior. As mentioned in the Introduction, the observed deviations from the scaling behavior at the AGS energies, have been attributed to the presence of collective expansion or

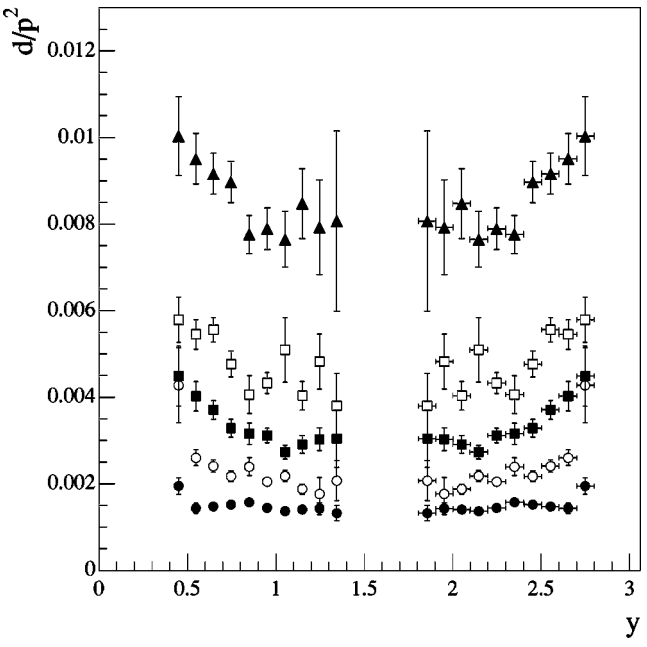

FIG. 16. dn/dy distributions for the deuterons divided by the square of the dn/dy distributions of the protons (d/p^2 ratio), as a function of the rapidity for different centrality cuts (as listed in Table I). The circles are for the 0–3 % centrality cut, the open circles are for the 12–17 % centrality cut, the squares are for the 24–32 % centrality cut, the open squares are for the 32–43 % centrality cut, and the triangles are for the 43–76 % centrality cut. The data points are reflected about mid-rapidity. The vertical error bars are statistical only; the systematic errors are discussed in the text.

transverse flow [6,28], and/or to the necessity of a third particle or a surrounding medium for coalescence [29,14].

Both the ''shoulder-arm shape'' of the differential cross sections and the evolution of the average transverse mass of the deuterons and the protons as a function of centrality observed in the data (Fig. 15), disagree with the simple thermal models that assume complete thermalization and coalescence. If it is assumed that the protons follow a Boltzmann distribution, that the deuterons are formed by simple coalescence, and the resulting $\langle m_t - m_0 \rangle$ for the deuteron will always fall below that of the proton, contrary to what is observed in the data. Moreover, the ''shoulder-arm shape'' of the differential cross sections and the difference between the average transverse mass of the deuterons and the protons as a function of centrality appear to be consistent, but it is not conclusive evidence of a scenario where the larger the mass of a particle, the larger the transverse momentum it gains from radial expansion [30]. It has been suggested [13] that the integration over transverse momentum of Eq. (1) should average out flow effects on the particle yield. In order to explore this yield scaling behavior, to first order, consider the experimental validity of a generalized coalescence picture using the following equation, with B_d a constant:

$$\frac{dn_d}{dy} = B_d \left(\frac{dn_p}{dy} \right)^2 . \tag{7}$$

Figure 16 shows the B_d or (d/p^2) as a function of the rapidity for different centrality cuts. The measured distributions follow a scaling behavior only for the three most central cuts, where the ratio remains constant as a function of the rapidity for the points with $y > 0.6$. For the other cuts, the d/p^2 has a strong dependence on y: d/p^2 decreases as one moves to midrapidity. The decreasing rate is larger for the less central cuts and for rapidity bins closer to the rapidity of the target and projectile.

A possible explanation for the d/p^2 dependence on the rapidity may be inferred from the deuteron yield. The shape of the rapidity distributions, in particular for the centrality cuts of 12–17 % and 24–32 %, suggest spectra composed of two components. One component is centered at midrapidity, predominantly the 0–3 % centrality cut, and is formed of deuterons from the participant region. The second component which is evident at low y close to the target rapidity grows larger for the more peripheral collisions, and may consist of deuterons from the target spectator that are not produced by coalescence. It is, thus, reasonable to assume that only the deuterons from the participant component may follow a scaling behavior.

The d/p^2 as a function of the centrality, $\langle n_{pp} \rangle$, for three rapidity bins is displayed in Fig. 17. Again, the d/p^2 distributions may be interpreted as composed of two components. The component from deuterons in the spectator region is mainly present at $\langle n_{pp} \rangle \leqslant 60$ and is larger at the lowest rapidity cut, and decreases at a fast rate as function of the centrality. The other component, from the participant deuterons is present at $\langle n_{pp} \rangle \geqslant 60$. It also decreases as a function of the centrality, but at a slower almost linear rate, and it is nearly independent of the rapidity cut. The evolution of the d/p^2 as a function of the $\langle n_{pp} \rangle$ of the participant component is then consistent with yield scaling: that is, it has a weak rapidity dependence and $d/p^2 \propto 1/V_{\text{source}}$ (since $\langle n_{pp} \rangle \propto V_{\text{source}}$), in agreement with a coalescence thermal model [27].

It is clear from Fig. 16 that the yield scaling behavior is observed only for the participant region of the distributions. Thus, the coalescence factor B_a from Eq. (1), that includes the transverse momentum dependence, is calculated only for the 0–3 % centrality cut. B_a is determined from the deuteron invariant spectra divided by the squared proton invariant spectra at $2m_t$ of the proton. B_a is presented in Table IV as a function of m_t and several rapidity bins. B_a is not constant either as a function of the rapidity or as a function of the transverse momentum as expected from a simple coalescence model.

It is common to present the interaction radius R, instead of B_a, which is defined by a thermal approximation [27,31]. According to this approximation, an estimate of the volume of the interaction region (V_{source}), is given as

$$B_a = A \frac{2s_A + 1}{2^A} R_{np}^N \frac{1}{N!Z!} \left[\frac{(2\pi\hbar)^3}{m_p V_{\text{source}}} \right], \tag{8}$$

where $A = 2$ is the deuteron atomic number, $s_A = 1$ the spin, R_{np}^N is the ratio of the total number of neutrons to protons in the system, and $N = 1$, $Z = 1$ is the neutron and proton number of the deuteron, and m_p is the rest mass of the proton.

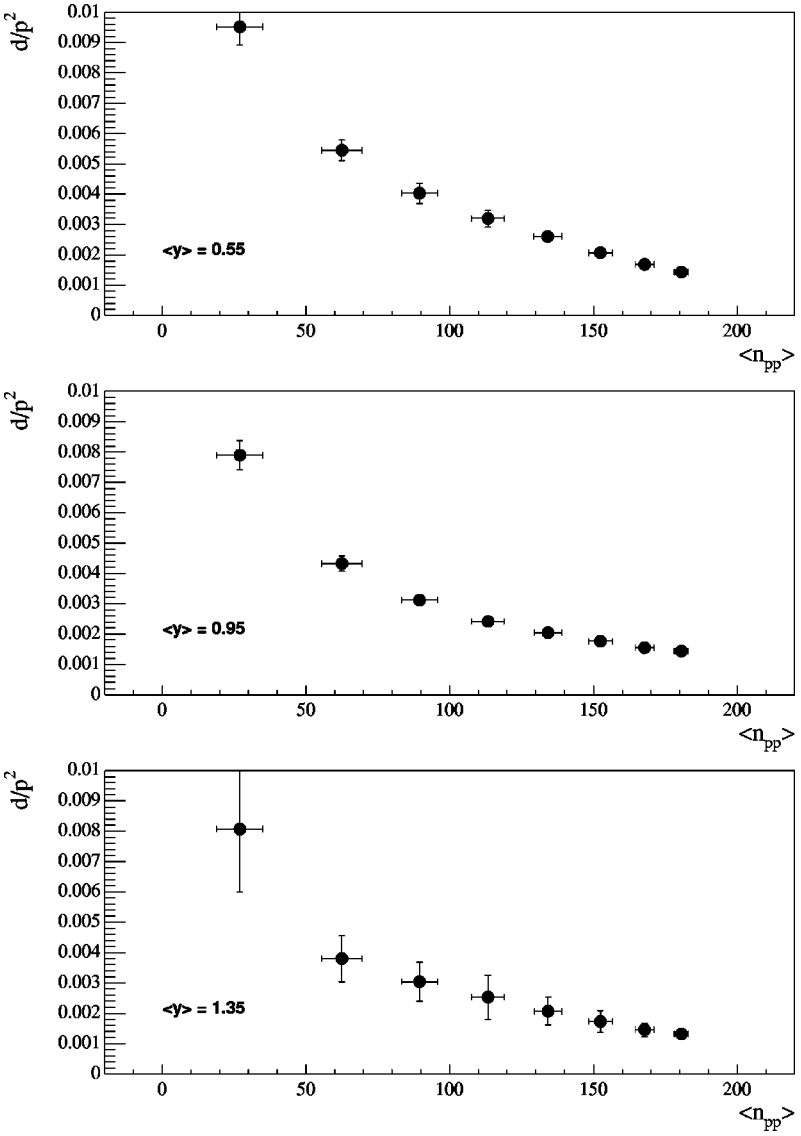

FIG. 17. The dn/dy distributions for the deuterons divided by the square of the dn/dy distributions of the protons (d/p^2 ratio), as a function of the number of projectile participants ($\langle n_{pp} \rangle$), for different, for three rapidity bins. The error bars are only statistical; the systematic errors are discussed in the text.

The interaction radius of the equivalent sphere can then be written as

$$R = \left(\frac{R_{np}^{N} 9 \pi^2 \hbar^3}{m B_a} \right)^{1/3}. \tag{9}$$

Figure 18 shows R as a function of the proton m_t for the 0–3 % centrality, and different rapidity bins. The values interaction radius shown in Fig. 18 are comparable with the average $R = 7.9 \pm 2$ fm, found for the central E-802 Si + Au system [2]. R decreases as a function of the transverse momentum for all the rapidities, and is smaller at a given transverse momentum for y closer to midrapidity.

The observation from Table IV that there remains a momentum dependence in the ratio of the deuteron spectra to the square of the proton spectra implies that either coalescence is not the mechanism by which the deuterons are formed or that there is a correlation between the momentum and the radial position of the nucleons at freeze-out [28]. One way to introduce this correlation is to assume a radial flow velocity which depends on the freeze-out radius. Unfortunately, measurements of the proton and deuteron spectra alone cannot constrain enough of the parameters, such as the nucleon density at freeze-out, the nucleon momentum profile in its local frame or the radial dependence of a flow velocity, to experimentally confirm coalescence as a unique interpretation. Nonetheless, there is the observed scaling in B_a. Detailed studies using cascade calculations [17,6], have shown that the transverse flow enhances the clustering volume, increases deuteron production, and removes the proportionality between the final deuteron momentum profile and the square of the nucleons. It would be helpful in this regard to examine the transverse momentum profile and scaling behavior of larger clusters and have measurements of directed transverse flow.

VI. CONCLUSIONS

In this paper the proton and deuteron $m_t - m_0$ distributions from the 11.6A GeV/c Au + Au reaction measured by the E802 Collaboration in 1994 are presented. The invariant double differential yields of protons and deuterons are not well-described by a single exponential fit in $m_t - m_0$. Rapidity distributions of dn/dy and the average transverse mass m_t are extracted from the distributions using a more general

TABLE IV. Coalesence factor B_a, the deuteron invarian spectra devided by the squared proton invariant spectra at 2 times m_t proton, for several rapidity bins. The errors cited are statistical only.

m_t (GeV)	B_a (GeV^2)	m_t (GeV)	B_a (GeV^2)
$0.4<y<0.5$ rapidity		$0.9<y<1.0$ rapidity	
1.025 ± 0.025	0.00078 ± 0.00003	1.025 ± 0.025	0.00059 ± 0.00004
1.075 ± 0.025	0.00059 ± 0.00004	1.075 ± 0.025	0.00070 ± 0.00002
1.125 ± 0.025	0.00085 ± 0.00005	1.125 ± 0.025	0.00082 ± 0.00004
1.175 ± 0.025	0.00074 ± 0.00008	1.175 ± 0.025	0.00081 ± 0.00005
$0.5<y<0.6$ rapidity		1.225 ± 0.025	0.00083 ± 0.00007
1.025 ± 0.025	0.00055 ± 0.00004	1.275 ± 0.025	0.00083 ± 0.00011
1.075 ± 0.025	0.00076 ± 0.00007	1.325 ± 0.025	0.00120 ± 0.00031
1.125 ± 0.025	0.00077 ± 0.00010	1.375 ± 0.025	0.00135 ± 0.00038
1.175 ± 0.025	0.00074 ± 0.00009	1.425 ± 0.025	0.00051 ± 0.00031
1.225 ± 0.025	0.00066 ± 0.00001	$1.0<y<1.1$ rapidity	
1.275 ± 0.025	0.00087 ± 0.00013	1.075 ± 0.025	0.00069 ± 0.00036
1.325 ± 0.025	0.00078 ± 0.00020	1.125 ± 0.025	0.00089 ± 0.00024
1.375 ± 0.025	0.00075 ± 0.00030	1.175 ± 0.025	0.00092 ± 0.00041
1.425 ± 0.025	0.00132 ± 0.00046	1.225 ± 0.025	0.00070 ± 0.00061
$0.6<y<0.7$ rapidity		1.275 ± 0.025	0.00081 ± 0.00009
1.025 ± 0.025	0.00061 ± 0.00001	1.325 ± 0.025	0.00068 ± 0.00011
1.075 ± 0.025	0.00057 ± 0.00007	1.375 ± 0.025	0.00091 ± 0.00014
1.125 ± 0.025	0.00077 ± 0.00009	1.425 ± 0.025	0.00119 ± 0.00026
1.175 ± 0.025	0.00092 ± 0.00013	1.475 ± 0.025	0.00129 ± 0.00034
1.225 ± 0.025	0.00070 ± 0.00016	$1.1<y<1.2$ rapidity	
1.275 ± 0.025	0.00074 ± 0.00016	1.075 ± 0.025	0.00078 ± 0.00006
1.325 ± 0.025	0.00103 ± 0.00025	1.125 ± 0.025	0.00101 ± 0.00007
1.375 ± 0.025	0.00101 ± 0.00026	1.175 ± 0.025	0.00077 ± 0.00003
1.425 ± 0.025	0.00072 ± 0.00032	1.225 ± 0.025	0.00102 ± 0.00007
1.475 ± 0.025	0.00089 ± 0.00038	1.275 ± 0.025	0.00076 ± 0.00007
$0.7<y<0.8$ rapidity		1.325 ± 0.025	0.00095 ± 0.00011
1.025 ± 0.025	0.00057 ± 0.00001	1.375 ± 0.025	0.00112 ± 0.00015
1.075 ± 0.025	0.00063 ± 0.00002	1.425 ± 0.025	0.00119 ± 0.00021
1.125 ± 0.025	0.00074 ± 0.00009	1.475 ± 0.025	0.00149 ± 0.00026
1.175 ± 0.025	0.00130 ± 0.00015	1.525 ± 0.025	0.00140 ± 0.00035
1.225 ± 0.025	0.00082 ± 0.00017	1.575 ± 0.025	0.00114 ± 0.00038
1.275 ± 0.025	0.00070 ± 0.00023	1.625 ± 0.025	0.00132 ± 0.00054
1.325 ± 0.025	0.00112 ± 0.00029	$1.2<y<1.3$ rapidity	
1.375 ± 0.025	0.00097 ± 0.00033	1.125 ± 0.025	0.00112 ± 0.00010
1.425 ± 0.025	0.00168 ± 0.00068	1.175 ± 0.025	0.00092 ± 0.00008
$0.8<y<0.9$ rapidity		1.225 ± 0.025	0.00123 ± 0.00007
1.025 ± 0.025	0.00049 ± 0.00002	1.275 ± 0.025	0.00098 ± 0.00008
1.075 ± 0.025	0.00077 ± 0.00002	1.325 ± 0.025	0.00084 ± 0.00009
1.125 ± 0.025	0.00075 ± 0.00004	1.375 ± 0.025	0.00115 ± 0.00012
1.175 ± 0.025	0.00113 ± 0.00012	1.425 ± 0.025	0.00149 ± 0.00019
1.225 ± 0.025	0.00063 ± 0.00015	1.475 ± 0.025	0.00163 ± 0.00027
1.275 ± 0.025	0.00099 ± 0.00025	$1.3<y<1.4$ rapidity	
1.325 ± 0.025	0.00094 ± 0.00034	1.175 ± 0.025	0.00092 ± 0.00013
1.375 ± 0.025	0.00036 ± 0.00023	1.225 ± 0.025	0.00100 ± 0.00015
1.425 ± 0.025	0.00163 ± 0.00043	1.275 ± 0.025	0.00131 ± 0.00020
1.475 ± 0.025	0.00140 ± 0.00083	1.325 ± 0.025	0.00139 ± 0.00011
		1.375 ± 0.025	0.00130 ± 0.00017

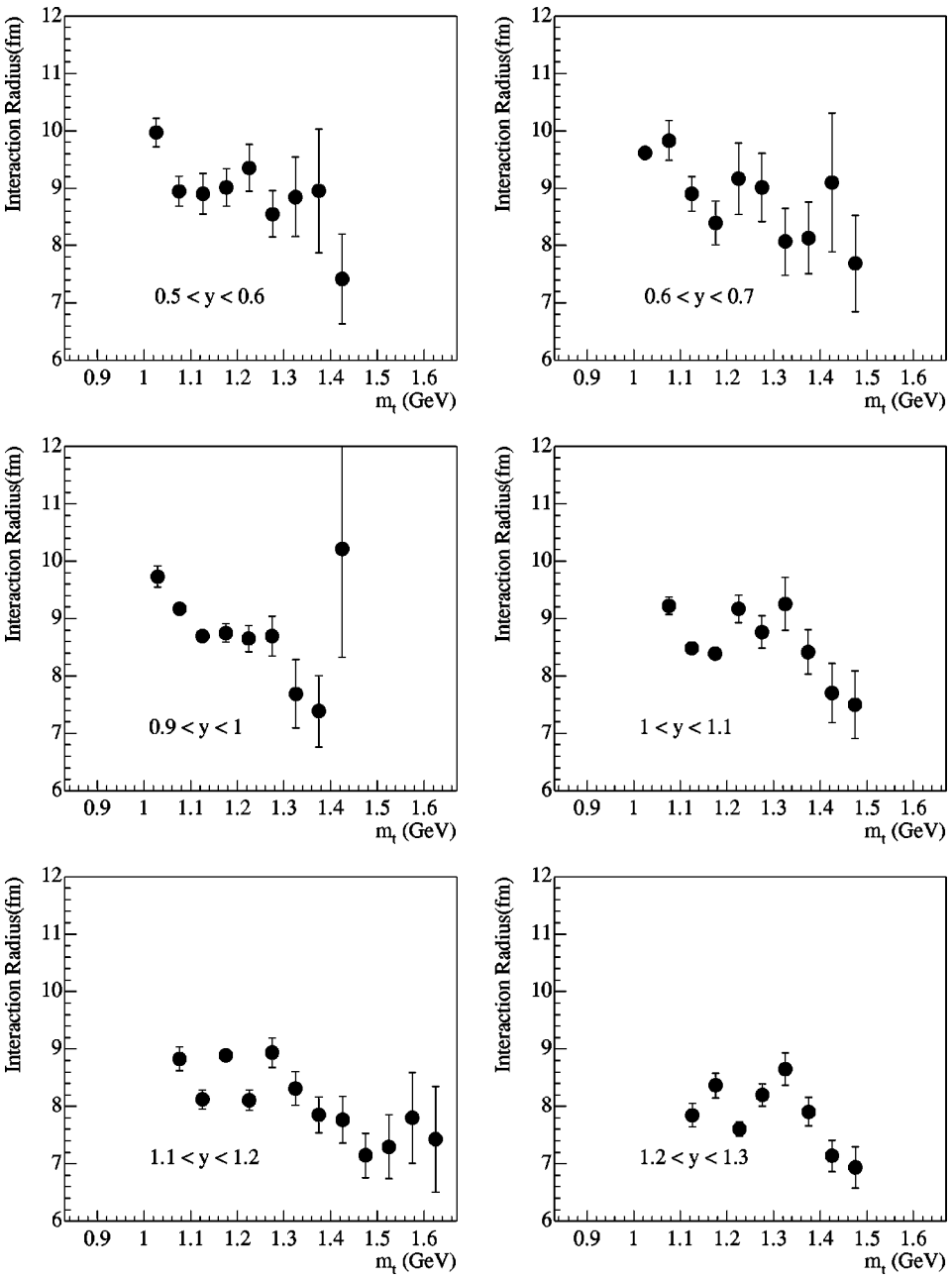

FIG. 18. Interaction radius R as a function of m_t, for six rapidity bins. The error bars are only statistical; the systematic errors are discussed in the text.

four-parameter function. The shoulder-arm shape of the cross sections and the evolution of the of the $\langle m_t \rangle - m_0$ as function of the centrality and rapidity are consistent but not conclusive evidence for radial expansion.

The production rate of deuterons as a function of rapidity satisfies a squared proton yield scaling behavior only for the more central cuts in centrality. The shape of the d/p^2 as a function of the rapidity and centrality may be explained if it is assumed that the yield of the deuterons is composed of two components, one from the spectator regions and the other from the participant region. That the d/p^2 is constant with rapidity for the participant region provides insight into the mechanism for coalescence. The decrease of the d/p^2 as a function of the $\langle n_{pp} \rangle$ indicates an increase in the size of the freeze-out volume and is evidence for a coalescence mechanism. For the most central cut, the evolution of the interaction radius (scaling factor B_a) as a function of $m_t - m_0$ and y may agree with a coalescence model in which the nucleons are affected by the correlations between the freeze-out volume and the transverse flow.

ACKNOWLEDGMENTS

This work was supported by the U.S. Department of Energy under contracts with BNL (DE-AC02-98CH10886), Columbia University (DE-FG02-86-ER40281), LLNL (W-7045-ENG-48), MIT (DE-AC02-76ER03069), UC Riverside (DE-FG03-86ER40271), University of Maryland (DOE-ER-404802), by NASA (NGR-05-003-513), under contract with the University of California, by the Ministry of Education and KOSEF (951-0202-032-2) in Korea, and by the Ministry of Education, Science, Sports, and Culture of Japan.

[1] L. Ahle *et al.*, E-802 Collaboration, Phys. Rev. C **57**, R466 (1998).
[2] T. Abbott *et al.*, E-802 Collaboration, Phys. Rev. C **50**, 1024 (1994).
[3] R. Stock, Phys. Rep. **135**, 259 (1986).
[4] T. Abbott *et al.*, E-802 Collaboration, Phys. Rev. Lett. **70**, 1393 (1993).
[5] J. Barrette *et al.*, E-877 Collaboration, Nucl. Phys. **A590**, 259c (1995).
[6] R. Mattiello, H. Sorge, H. Stöcker, and W. Greiner, Phys. Rev. C **55**, 1443 (1997).
[7] S. V. Afanasjev *et al.*, NA49 Collaboration, Nucl. Phys. **A610**, 76c (1996).
[8] D. E. Kahana *et al.*, Phys. Rev. C **54**, 338 (1996).
[9] S. Chapman and R. Nix, Phys. Rev. C **54**, 866 (1996).
[10] A. Schwarzschild and C. Zupancic, Phys. Rev. **129**, 836 (1963).
[11] L. P. Csernai and J. I. Kapusta, Phys. Rep. **131**, 131 (1986).
[12] J. Barrette *et al.*, E-814 Collaboration, Phys. Rev. C **50**, 1077 (1994).
[13] H. Sorge, J. L. Nagle, and B. S. Kumar, Phys. Lett. B **355**, 27 (1995).
[14] S. Leupold and U. Heinz, Phys. Rev. C **50**, 110 (1994).
[15] P. Danielewicz and G. F. Bertsch, Nucl. Phys. **A533**, 712 (1991).
[16] H. Sorge, H. H. Stöcker, and W. Greiner, Ann. Phys. (N.Y.) **192**, 266 (1989).
[17] R. Mattiello, A. Jahns, H. Sorge, H. Stöcker, and W. Greiner, Phys. Rev. Lett. **74**, 2180 (1995).
[18] T. Abbott *et al.*, E-802 Collaboration, Nucl. Instrum. Methods Phys. Res. A **290**, 41 (1990).
[19] R. Debbe *et al.*, Nucl. Instrum. Methods Phys. Res. A **403**, 256 (1998).
[20] T. Sugitate, Y. Akiba, S. Hayashi, Y. Miake, S. Nagayima, and M. Torikoshi, Nucl. Instrum. Methods Phys. Res. A **249**, 354 (1986).
[21] D. Beavis, R. R. Betts, M. A. Bloomer, Y. Y. Chu, J. B. Cumming, E. Duek, P. E. Haustergin, I. Juricic, S. Katcoff, and S. B. Kaufman, Nucl. Instrum. Methods Phys. Res. A **281**, 367 (1989).
[22] L. Ahle, Ph.D. thesis, M.I.T., 1997.
[23] R. Brun *et al.*, GEANT user guide, Report DD/EE/84-1, CERN 1987.
[24] L. Ahle *et al.*, E-802 Collaboration, Phys. Rev. C **57**, 1416 (1998).
[25] MINUIT reference manual, version 92.1, D506 CERN, 1992.
[26] L. Ahle *et al.*, E-802 Collaboration, Nucl. Phys. **A590**, 249c (1995).
[27] S. Das Gupta and A. Z. Mekjian, Phys. Rep. **72**, 131 (1981).
[28] A. Polleri *et al.*, Phys. Lett. B **419**, 19 (1998).
[29] S. Mrówczyński, Phys. Lett. B **308**, 216 (1993).
[30] P. J. Siemmens and J. O. Rasmussen, Phys. Rev. Lett. **42**, 880 (1979).
[31] J. L. Nagle, B. S. Kumar, D. Kusnezov, H. Sorge, and R. Mattiello, Phys. Rev. C **53**, 367 (1996).